Fuel 251 (2019) 328–340

Contents lists available at ScienceDirect

Fuel

journal homepage: www.elsevier.com/locate/fuel

Full Length Article

Promoting “adiabatic core” approximation in a rapid compression machine by an optimized creviced piston design

Yingtao Wu[a], Meng Yang[a], Chenglong Tang[a,*], Yang Liu[a], Peng Zhang[b], Zuohua Huang[a]

[a] State Key Laboratory of Multiphase Flow in Power Engineering, Xi'an Jiaotong University, Xi'an 710049, China
[b] Department of Mechanical Engineering, The Hong Kong Polytechnic University, Hung Hom, Kowloon, Hong Kong

ARTICLE INFO

Keywords:
Rapid compression machine (RCM)
Creviced piston
Adiabatic core
Temperature homogeneity
Ignition delay time

ABSTRACT

Rapid compression machine (RCM) is a widely-used experimental instrument for measuring ignition delay time (IDT) in the low-to-intermediate temperature range. In this work, to enhance the validity of the “adiabatic core” approximation in RCM, a piston crevice for suppressing the piston-driven vortex and therefore promoting the temperature homogeneity in the combustion chamber was firstly optimized by numerical simulation with a dynamic mesh strategy. Results show that crevice volume should be large enough to contain most of the boundary layer cold gas during the compression so as to assure the temperature homogeneity in the reaction chamber. While the shape of the crevice (with sufficiently large volume) only weakly affects the temperature homogeneity. An optimized piston was tested across wider ranges of pressure, the chamber length, and inert gas under experimental conditions. Based on the optimized piston crevice, a RCM was established and tested. Test results have confirmed that the crevice shape does not affect the IDT measurements, provided the crevice volume fixed. In addition, the present IDTs show consistency with those using other RCMs, as well as with the numerical predictions obtained by using the well-recognized and validated kinetic mechanisms, which support the validity of the present RCM facility for ignition delay measurement.

1. Introduction

Ignition delay time (IDT) of a reactive gas mixture is a fundamental combustion parameter, which reflects the thermochemical and chemical kinetic characteristics of the mixture. Theoretically, the IDT is defined as the duration from the time instant when a perfectly-mixed fuel and oxidizer is brought to a thermodynamic state with a certain initial condition to the time instant when a thermal runaway (or/and radical runaway) occurs in the system. The thermal runaway (or radical runaway) is characterized by the rapid increase of the temperature (or the concentrations of radicals for chain reactions). IDT is typically measured by using the shock tube [1–3] and rapid compression machine (RCM) [4–8]. Shock tube generates a nearly constant-pressure environment behind the reflective shock wave, and the time zero for the auto-ignition of the gas mixture is well-defined as the instant when the incident shock wave arrives at the end wall. Due to the limitation of the effective testing time, shock tube is particularly suitable when the IDT is sufficiently short at high temperatures (> 1000 K) [9]. RCM mimics the compression stroke and the subsequent constant-volume combustion for a piston-cylinder assembly in internal combustion engines. At the end of compression (EOC), the piston of RCM is locked and provides a nearly constant-volume environment for the auto-ignition. Compared with shock tube, RCM can generate a long-lasting environment suitable for relatively long IDTs in the low-to-intermediate temperature range. Recently, RCMs have also been used for intermediate species measurements during auto-ignition [10–13].

The conventional analysis of RCM experiments assumes the auto-ignition occurs in a homogeneous, adiabatic, constant-volume reaction chamber, in which there are no bulk flow and mass and heat transfer. The pressure signal in the reaction chamber can be obtained through pressure transducer with high sampling frequency, and temperature is calculated from the pressure profile. Considering that the practical compression process unavoidably induces heat loss through chamber walls, an “adiabatic core hypothesis” [14] is typically used in calculating the temperature (T_c) at the EOC. The hypothesis states that the core region of the reaction chamber is considered as adiabatic and it would be affected by the expansion due to the heat loss that affects the other parts of the test volume. Based on this hypothesis, T_c is calculated by

$$\int_{T_0}^{T_c} \frac{\gamma}{\gamma - 1} \frac{dT}{T} = \ln\left(\frac{P_c}{P_0}\right) \tag{1}$$

* Corresponding author.
E-mail address: chenglongtang@mail.xjtu.edu.cn (C. Tang).

https://doi.org/10.1016/j.fuel.2019.04.030
Received 11 January 2019; Received in revised form 30 March 2019; Accepted 4 April 2019
Available online 13 April 2019
0016-2361/

where T and P are the temperature and the pressure, the subscripts "0" and "c" indicate the initial and the EOC times, and γ is the temperature-dependent specific heat ratio.

Previous studies [15–17] have shown that the motion of the flat piston during compression could create roll-up vortices in front of the piston head with enhanced mixing between the colder gases in the boundary layer and hotter gases in the core region, tending to deteriorate the validity of the "adiabatic core" hypothesis [18]. For chemical kinetic research, studies have highlighted the effect of creviced piston design in reducing the temperature inhomogeneity [15] by suppressing the formation of the vortices. Specifically, Würmel and Simmie [16] numerically simulated the temperature field in a twin-piston RCM to investigate the influences of piston crevice volume, location, channel size, and inert gases (oxygen, nitrogen, xenon and helium). Mittal and Sung [17] used a planar laser-induced fluorescence (PLIF) technique to investigate the effect of the piston with/without crevice and found that a creviced piston design drastically reduces the vortex formation and leads to increased temperature homogeneity. In addition, they compared the experimental results with the simulations based on different flow models and found that the simulation results using the laminar model agrees better with the experimentally resolved temperature field.

Mittal et al. [18,19] numerically simulated hydrogen ignition in a RCM to validate the "adiabatic core" hypothesis. They found that the homogeneity of the temperature field could be promoted for higher pressure, shorter stroke length and larger reaction chamber. Although a large piston crevice can suppress the vortices more effectively, it however brings in more complex influences to the experimental results in multi-stage ignition process [19–22]. When the first-stage ignition occurs, pressure increases in the core region and some hot gas will flow into the crevice. As a result, the pressure for the second-stage ignition is actually lower than that of the case with flat piston. To resolve such a pressure drop in the second-stage ignition, Goldsborough and co-workers [20] developed a multi-zone model (MZM) to simulate the multi-stage ignition in RCM. Mittal et al. proposed a "crevice containment" design [21,22], which is expected to suppress the roll-up vortices and to avoid the crevice effects during multi-stage ignition. In such a design, a seal ring between the piston and the chamber wall could block the channel between the reaction chamber and the crevice and therefore prevent the hot gas from flowing into the crevice. It should be noted that this is a quite challenging design because of the technical difficulty of the sealing and because the crevice containments need to be changed from time to time. Recently, Bourgeois et al. [23] developed a method to validate piston crevice design under various operating conditions by predicting a critical mass that needs to be tracked in the crevice volume and assessing whether a specific crevice volume can track this mass during the compression. This method could be able to ensure temperature homogeneity at EOC, however, it has not been tested across the typically time range that a RCM is operated.

Regardless of the previous studies that advance the optimization of RCM piston design, the effects of the crevice geometry on promoting the "adiabatic core" approximation have not been fully explored yet and have not been experimentally validated. Distinct from the RCMs in above literature, this RCM has a long stroke length (332 mm) and reaction chamber length (30–100 mm), and therefore it is also interesting to recheck these parameter effect in the current configurations. In the present study, we first numerically investigated the crevice geometry (volume and shape) effects on the temperature inhomogeneity in the reaction chamber after EOC, with particular emphasis on conducting parametric study to obtain an optimal piston crevice design with minimal temperature inhomogeneity. We note that for the numerical simulation of the flow in the rapid compression machine, previous work typically adopts the dynamic mesh method [17,19,24]. However, there are only limited discussions on the dynamic mesh strategy used in the CFD simulation. This work, therefore, has included a detailed discussion on the dynamic mesh strategy especially on the moving boundary location. Secondly, the optimized crevice design is then validated against different compression pressure and chamber length. In addition, we note that Argon is a commonly used insert gas in RCM experiment [16]. However, the temperature distribution of argon is missing in the previous study. We will additionally test the optimized crevice design against different inert gases by comparing the temperature distribution of argon with that of nitrogen under the same condition [16]. Finally, by use of a newly established RCM based on the design, we validated the IDT measurement of typical reactive mixtures against its modeling based the widely-accepted reaction mechanism and the IDT measurements of other RCMs. The study substantiates that auto-ignition of various fuels can be conducted in this facility, which will provide reliable data for modeling combustion chemistry in the low-to-intermediate temperature range in the future.

2. CFD-assisted design of creviced piston

2.1. CFD specifications

2.1.1. Computational domain and model selection

The geometry of the piston crevice to be optimized and the mesh at EOC are shown in Fig. 1. Piston crevice is characterized by lengths d and e, as shown in Table 1. Pistons #0 to #3 were compared to explore the crevice volume effect on the temperature homogeneity; piston #0 is a baseline flat piston. A dimensionless ratio ($V_{cr}/\pi R^2 S$), proposed by Yousefian et al. [24], is used to measure the relative significance of the crevice volume V_{cr} compared with the piston swept volume, where R is the radius of the combustion chamber (25.4 mm), S is the piston stroke 330 mm. Piston #3 and #4 have the same crevice volume but different shapes so that the crevice shape effect can be addressed.

The mesh generation for the axis-symmetric computational domain was conducted by using the ICEM-CFD software [25], and quadrilateral

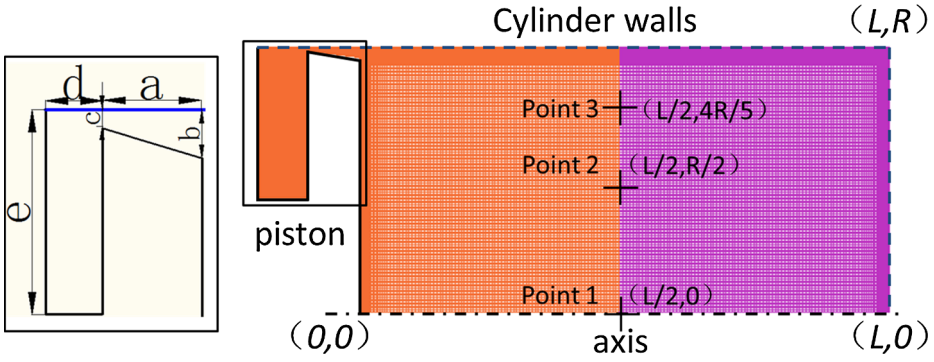

Fig. 1. The geometry and mesh of the crevice and reaction chamber. R is radius of the reaction chamber (25.4 mm), and L is the reaction chamber length after EOC (three test cases: 30, 50 and 100 mm).

Table 1
Geometry parameters for pistons #0 to #4.

Crevice#	a (mm)	b (mm)	c (mm)	d (mm)	e (mm)	V_{cr} (mm^3)	$V_{cr}/\pi R^2 S$
0	0.0	0.0	0.0	0.0	0.0	0.00	0.000
1	4.0	1.0	0.4	2.0	14.5	3305.48	0.005
2	4.0	1.0	0.4	4.6	14.5	7602.60	0.011
3	4.0	1.0	0.4	8.0	14.5	13221.91	0.020
4	4.0	1.0	0.4	19.0	4.8	13172.93	0.020

mesh with layering method was used in the dynamic mesh modeling [19,24]. The computational domain is divided into two zones including one near the piston and one far away from it, which will be discussed in detail in Section 2.1.2. During the compression, the mesh in the near piston zone remains unchanged while the mesh layers in the far away zone are merged so that the dynamic mesh is realized. In this work, the minimum (maximum) cell size is 0.02 mm (0.3 mm) in the axis direction and 0.006 mm (0.18 mm) in the radial direction after EOC, while slightly larger cells (the maximum size in the axial direction is 0.5 mm) are used in the compressed mesh part (the far away mesh zone) to reduce the computational load. By using the FLUENT software package [26], the flow and temperature fields during the compression process was simulated to compare different crevice geometries. The simulation includes the entire process of compression and 150 ms after EOC, and this time scale covers typical reliable range of IDT measurement by using the rapid compression machine. The total number of grids varies from 100,000 to 700,000 during the compression. Grid independent study has been conducted to justify the present mesh, which is more refined than those used in the previous simulations [16–19,21,22,24].

As discussed in the introduction, laminar flow simulation was found to be more suitable for the RCM flow after EOC [17–19,21,27]. A Reynolds number of the RCM flow can be defined by $Re = U_c L/\nu$, where the characteristic flow velocity should be smaller than the average piston moving velocity $U_c = \frac{S}{t_{EOC}} = 8.25$ m/s, where the piston stroke S is 330 mm, and the compression time t_{EOC} is 40 ms. Considering that the pressure remains nearly constant after EOC, we have $\rho_c/\rho_0 \sim T_0/T_c$ from the ideal gas law and $\mu/\mu_0 = \left(\frac{T_C}{T_0}\right)^{\frac{3}{2}} \frac{T_0 + T_S}{T_C + T_S}$ from the Sutherland's law [28], and therefore have $\nu/\nu_0 = \left(\frac{T_C}{T_0}\right)^{\frac{5}{2}} \frac{T_0 + T_S}{T_C + T_S}$, where T_S is the Sutherland temperature (for air, $T_s = 110$ K), T_0 is the reference temperature 300 K, $\nu_0 = 15.69 \times 10^{-6}$ m^2/s is the kinematic viscosity of air at T_0, and the typical temperature after EOC T_c is in the range between 700 and 1000 K. Applying all the values, the dynamic Reynolds number varies around 2000–4000, which indicates that the flow pattern resides in the transition region. In addition, Yousefian et al. [27] recently compared the 3D Large Eddy Simulation (LES) and the 2D laminar model and showed that the temperature inhomogeneity resolved by these two methods agrees satisfactorily under all conditions. As such, laminar flow simulation is used in this work to facilitate the present parametric study for optimization design.

Nitrogen is selected as the testing gas for most of the cases using ideal gas model and polynomials for constant-pressure specific heat, thermal conductivity and dynamic viscosity coefficient. Fixed temperature (300 K) and no-slip boundary conditions are set to all solid surfaces. The piston moving profile as the function of time is deduced from the experimentally measured pressure trace (provided in the Supplementary material).

PISO (Pressure-Implicit Split-Operator) algorithm is used for the pressure-velocity coupling, PRESTO (Pressure Staggering Option) scheme for pressure, and the second-order upwind discretization for density, momentum, and energy. The residuals of continuity and energy are 10^{-4} and 10^{-6} respectively. The time step is set to be 20 μs to better resolve the temperature and flow development in the reaction chamber.

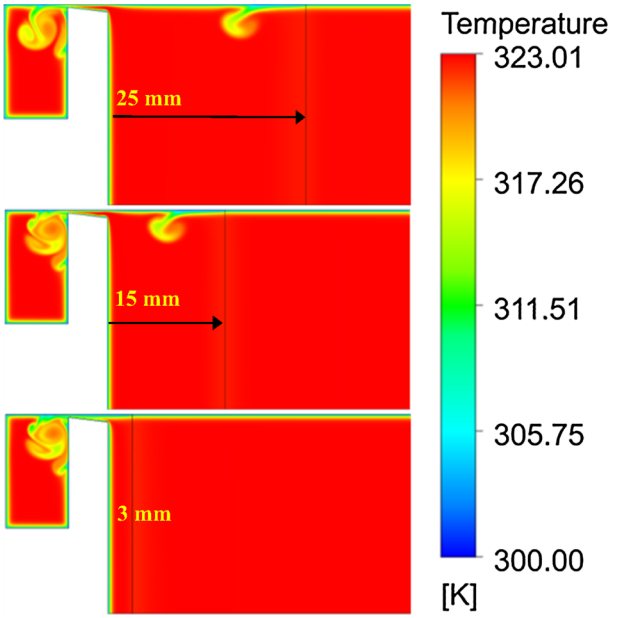

Fig. 2. The temperature distributions in the reaction chamber with different locations of the moving boundary (25, 15 and 3 mm between the piston surface) in the dynamic mesh strategy at −25 ms (25 ms before the end of compression); PC = 30 bar; N2; L = 30 mm.

2.1.2. Dynamic mesh strategy: discussion on the moving boundary location

In order to simulate the compression process in the RCM, layering dynamic mesh method has been typically used to realise the mesh movement [17,19,24]. By using this method, a cell layer next to the moving boundary will be split or merged with the adjacent cell layer when the height of this layer has reached the split factor or collapse factor specified. This dynamic method will change the boundary layer cell height when it is moving. However, the near-wall cell is usually densified to better capture the fluid dynamics in this region, which requires that the first cell layer near the wall should be very small and the layer height far from the wall increases at a certain ratio. If the moving boundary is setting as the real boundary in the combustion chamber which is the piston surface, the densified cells near the piston surface will be destroyed during its movement. Because the fluid dynamic near walls is of great importance, the moving boundary is typically set outside the boundary layer. This method is adopted in this work, as also used in reference [24]. Therefore, locations of the moving boundary in the dynamic mesh strategy have been investigated.

As shown in Fig. 2, we have set different three different moving boundary layer locations, 25, 15 and 3 mm respectively above the piston surface. It is seen that disturbances of cold boundary gas are observed behind the moving boundary for cases 25 mm and 15 mm, and this would lead to extra deterioration of temperature homogeneity in the main chamber zone. This is because the gas containing cells behind the moving boundary are moving with the piston and create a velocity gradient with the static gas within the viscous boundary layer, resulting in vortex diffusion shown in the figure When the moving boundary layer is close to the piston surface as shown in the third row, the cold gas disturbance is directly transported into the crevice and thus will not influence the temperature field in the main chamber zone. In addition, the location of the moving boundary is also affected by the cell height. If the cell height in the moving boundary is too small (close to the piston surface), negative volume cell error is more likely to occur during the mesh movement, or shorter time step should be adopted which will increase the computation cost. Therefore, in this study, the moving boundaries are located in 3 mm from the piston surface where no extra disturbance will occur and the cell height has been fully developed (0.3 mm) for all the simulation in the following sections.

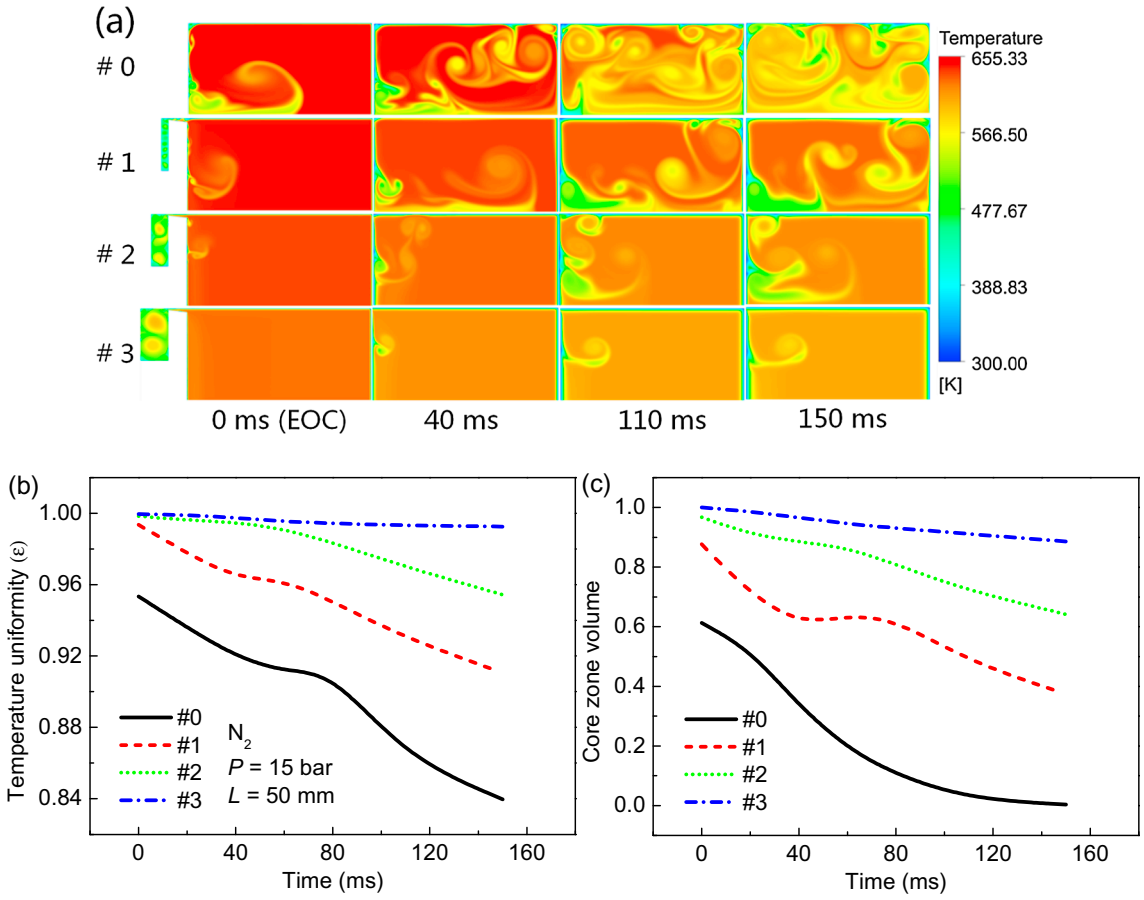

Fig. 3. (a) Temperature distributions for #0, #1, #2 and #3 piston at different times; (b) Temperature uniformity variable for #0, #1, #2 and #3 piston as a function of time; (c) Core zone volume for #0, #1, #2 and #3 piston as a function of time; P_C = 15 bar; N_2; L = 50 mm.

2.2. Effect of the piston crevice volume

We have firstly performed non-reactive simulations for piston #0, #1, #2, and #3 with different lengths of d (see Fig. 1) and hence different volumes, such that an approximately nearly-optimized crevice volume could be determined by the comparison. Fig. 3(a) shows the temperature distribution with increased piston crevice volume for the period between EOC and 150 ms after EOC. This period is long enough to cover the measured IDTs range of typical IDTs measured by RCMs [4,5]. Pressure at EOC (*Pc*) is fixed around 15 bar for all the pistons, so that pressure variation effect on the temperature homogeneity could be eliminated. It is seen that temperature in the reaction chamber is not complete uniformly distributed for any of the cases throughout this entire period and that the gas mixing between the core and boundary layer is more intense as time proceeds. However, more homogeneous temperature field and smaller vortex scale can be observed as the crevice volume increased. For piston #1 and #2, a cold gas plug shows up and penetrates to the center region in a short interval after EOC and the hot gas becomes restricted to a toroidal region surrounding the cold core. A similar phenomenon was also experimentally observed by Griffiths et al. [29] and Clarkson et al. [30], who suggested that the conventional homogeneous model still appears to be robust under such a temperature field. For piston #3, the temperature distribution is very homogeneous and only a small scale of disturbance was occurred on the piston head from 40 ms to 150 ms.

To further quantify the temperature inhomogeneity, a mass averaged temperature within the reaction chamber $T_{ave}(t)$ was calculated by

$$Tave = \frac{\sum T_i \rho_i}{\sum \rho_i} \quad (2)$$

where i is the cell number in the mesh, T_i and ρ_i are the time-dependent temperature and density within the cell respectively. The mass-averaged temperature $T_{ave}(t)$ quantitatively represents the temperature in the reaction chamber subject to mixing and flow. The temperature in the piston crevice and a boundary layer of 3 mm are not included in the calculation because they do not influence the ignition process. We then define a temperature uniformity variable ε as

$$\varepsilon = \frac{T_{ave}(t) - T_w}{T_{max}(t) - T_w} \quad (3)$$

where $T_{max}(t)$ is the maximum temperature in the reaction chamber at a specific instant, and T_w is the wall temperature. $T_{max}(t)$ has been carefully compared with the temperature calculated from adiabatic compression theory ($T_{adiabatic}(t)$), and deviations between $T_{max}(t)$ and $T_{adiabatic}(t)$ are within 0.5 K for all the cases studied (details of the comparison are provided in the Supplementary material). If ε is close to 1, $T_{ave}(t)$ is close to $T_{max}(t)$, indicating that the average temperature in the reaction chamber is close to the "adiabatic core hypothesis" temperature $T_{adiabatic}(t)$. Thus ε is a physically meaningful variable in quantifying the temperature uniformity after EOC. Similar definitions have also been used by the previous studies [19,24].

However, definition of ε does not distinguish the contributions of the thermal boundary layer growth and the cold gas vortex to the overall level of temperature homogeneity, as also stated in reference [23]. Therefore, another dimensionless definition of "core zone volume" was also used as an assistant criterion in comparing the adiabatic core for all the studied cases. Core zone volume is defined as the density weighted volume of the core zone gas ($T > T_{adiabcore} - 5$ K) to the total density weighted volume of main chamber zone (crevice and a boundary layer of 3 mm were not included). Thus, the dimensionless

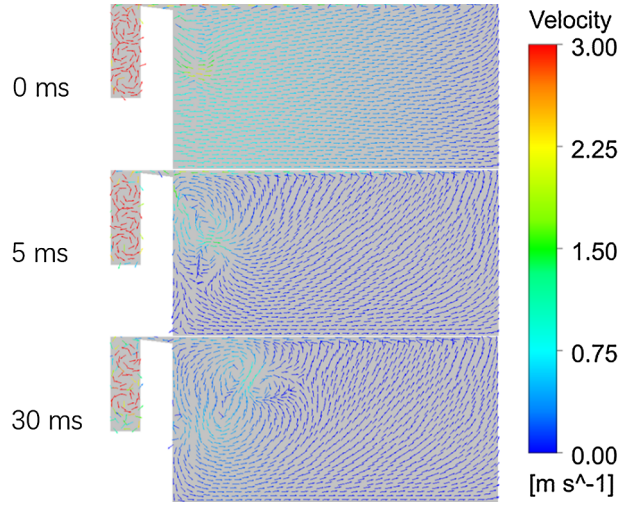

Fig. 4. Vortexes transport within the reaction chamber of piston #3, P_C = 15 bar, L = 50 mm.

core zone volume can reflect the percentage of the gas that is unaffected by the cold disturbances in the main chamber zone.

The time histories of ε for piston crevice #0 to #3 are shown in Fig. 3(b). For all the piston crevices, ε shows a decaying trend because of the progressively increased mixing between the boundary layer and the core region. Additionally, ε with increased crevice volume shows significantly slower rate of decaying, indicating an increased level of temperature uniformity for larger piston crevice volume. Similar trend has been observed in the core zone volume as a function of time, as shown in Fig. 3(c). For flat piston #0, only about 60% core zone volume is existed at EOC and it shrinks very fast that there was almost no core zone at 150 ms. On the contrary, core zone volume of piston #3 is 100% at EOC and still around 90% even at 150 ms. Piston #3 shows very slow rate of decline in both Fig. 3(b) and (c), indicating that a well-defined adiabatic core is existed in the chamber for entire period.

The results shown in Fig. 3 can be further explained by investigating the flow field. As shown in the Fig. 4, initially the roll-up vortexes are generated from the boundary layer of the reaction chamber wall or the piston surface due to the piston motion. As piston keeps moving, these vortexes tend to be transported into the core region of the reaction chamber or into the crevice through the channel. When the volume of the crevice is not large enough to accommodate the swept boundary layer gas, vortexes are generated from the chamber wall and the piston surface and further mix with the core region charge, which induce significant temperature inhomogeneity. With the increase of the piston crevice volume, the temperature distribution in the reaction chamber after EOC becomes increasingly uniform. We note that as the crevice volume is increased, more cool gas is trapped in the crevice and less is remained in the reaction chamber during the compression process. Thus, there is less vortex mixing within the core region for larger crevice volume.

2.3. Assessment of "adiabatic core" by temperature history

The "adiabatic core" hypothesis, which is used to estimate the highest temperature in the reaction chamber, is more appropriate to validate chemical kinetic models when this core zone is large and homogeneous. However, the temperature field in the core zone is unnecessary to be absolute homogeneous to create an "adiabatic core". Experimental and numerical studies [18,29,30] were focused on the auto-ignition in a stratified temperature field and showed that the adiabatic compressed core gas dominates the rate development of reactions, which determines the IDT even when there is spatial

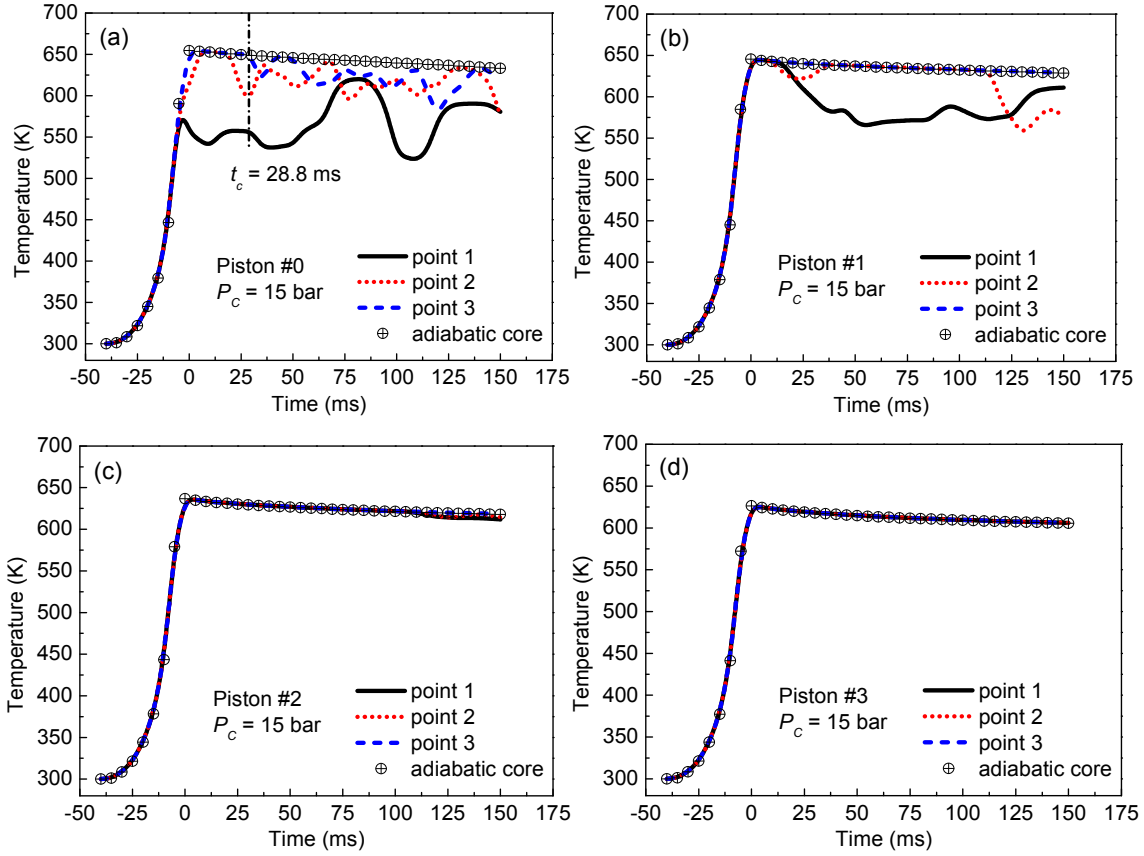

Fig. 5. Temperature discrepancy with the adiabatic core hypothesis at different points for piston #0 (a), #1 (b), #2 (c) and #3 (d); L = 50 mm. P_C = 15 bar; N_2.

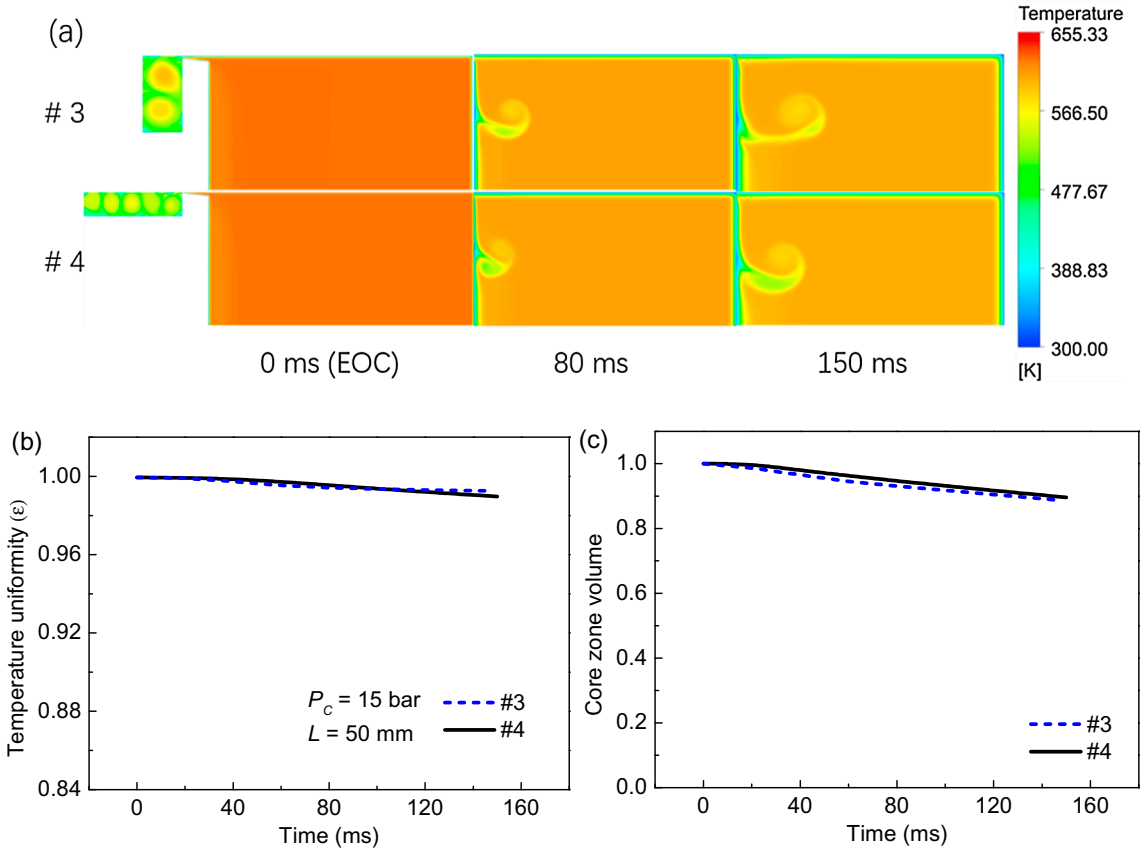

Fig. 6. (a) Temperature distributions at 0, 80 and 150 ms for pistons #3 and #4; (b) Temperature uniformity variable for piston #3 and #4 as a function of time; (c) Core zone volume for piston #3 and #4 as a function of time; P_c = 15 bar and L = 50 mm, N_2 as the bulk gas.

inhomogeneity. While in a negative temperature dependent regime, the temperature inhomogeneities tends to be smoothed out during the auto-ignition. Thus, for the IDT study, it is more reasonable to validate the "adiabatic core" hypothesis against the temperature history in the hot core region.

For the flat piston (#0), the hot core region exists for a short period of time after EOC. But as the time proceeds, the cold gas then mixes with the hot gas in the region due to the vortex so that the hot core region shrinks and eventually vanishes. For a larger piston crevice, such as #3, the vortex in the chamber is very weak, and an obvious hot core region exists even at 150 ms after EOC. In order to quantitatively evaluate the discrepancy between the hot core temperature and the "adiabatic core" temperature, the temperature history profiles of three typical points (point 1, point 2 and point 3, as shown in Fig. 1) are compared with the temperature histories derived from "adiabatic core" hypothesis, as shown in Fig. 5. These three points are in the center of the reaction chamber over radial direction, which can represent most of the core region that is less likely to be disturbed by the cold boundary layer gas according to the temperature contours.

For the flat piston #0, point 1 and point 2 show discrepancies at the very beginning of the heat loss process, and the temperature continues to fluctuate, indicating that a stable hot core cannot be established. However, the temperature at point 3 is consistent with the adiabatic core temperature until the time of 28.8 ms (t_c), and then the hot core is disturbed by mixing with cold gas. As the crevice volume increases, the temperature histories of these points are consistent with the adiabatic core temperature for a longer time, and the extent of temperature fluctuation at point 2 and point 1 is decreased, indicating that the hot core region not only lasts longer but also becomes bigger. In actual RCMs, both spontaneous ignition and flame propagation exist [31–33], and the latter is more flavored to happen for a hotspot zone surrounded by large temperature gradient. Inhomogeneous temperature distribution in the reaction chamber will also lead to abnormal combustion behaviors such as strong knocking, in which the gas is first ignited in multiple hotspots and then followed by different mode of propagation [33,34]. If more mixture is reacted through flame propagation, the steep pressure increase caused by ignition of the gas mixture will be postponed and thus increases the measured IDT. Consequently, a bigger hot core can lead to a more accurate IDT measurement.

2.4. An optimized piston crevice

2.4.1. Test against different crevice shape

We showed in the previous section that if the piston volume is large, the temperature homogeneity in the reaction chamber will be better. For piston crevices with the same enough large volume, the crevice may still have different shapes. Some of them are "narrow and deep" structured while others are "wide and shallow" [16]. We then tried to see if the crevice shape may influence the vortex formation and therefore the flow uniformity in the chamber.

For the pistons #3 and #4, the crevice volume is fixed, while the crevices of them are respectively "narrow and deep" and "wide and shallow". Temperature distributions at EOC, 80 and 150 ms are shown in Fig. 6(a). It is seen that the temperature distributions in the reaction chambers are very identical for the pistons #3 and #4 at different times. Also, a crevice with larger aspect ratio (e/d or d/e) is better at cooling the trapped gases. For utilizing the creviced piston, the crevice volume is the essential factor in design and should be large enough to contain most of the boundary layer gases. However, these mixtures in the crevice does not necessarily influence the temperature uniformity inside the main reaction chamber. As shown in Fig. 6(b) and (c), the temperature uniformity parameter ε and core zone volume of these two

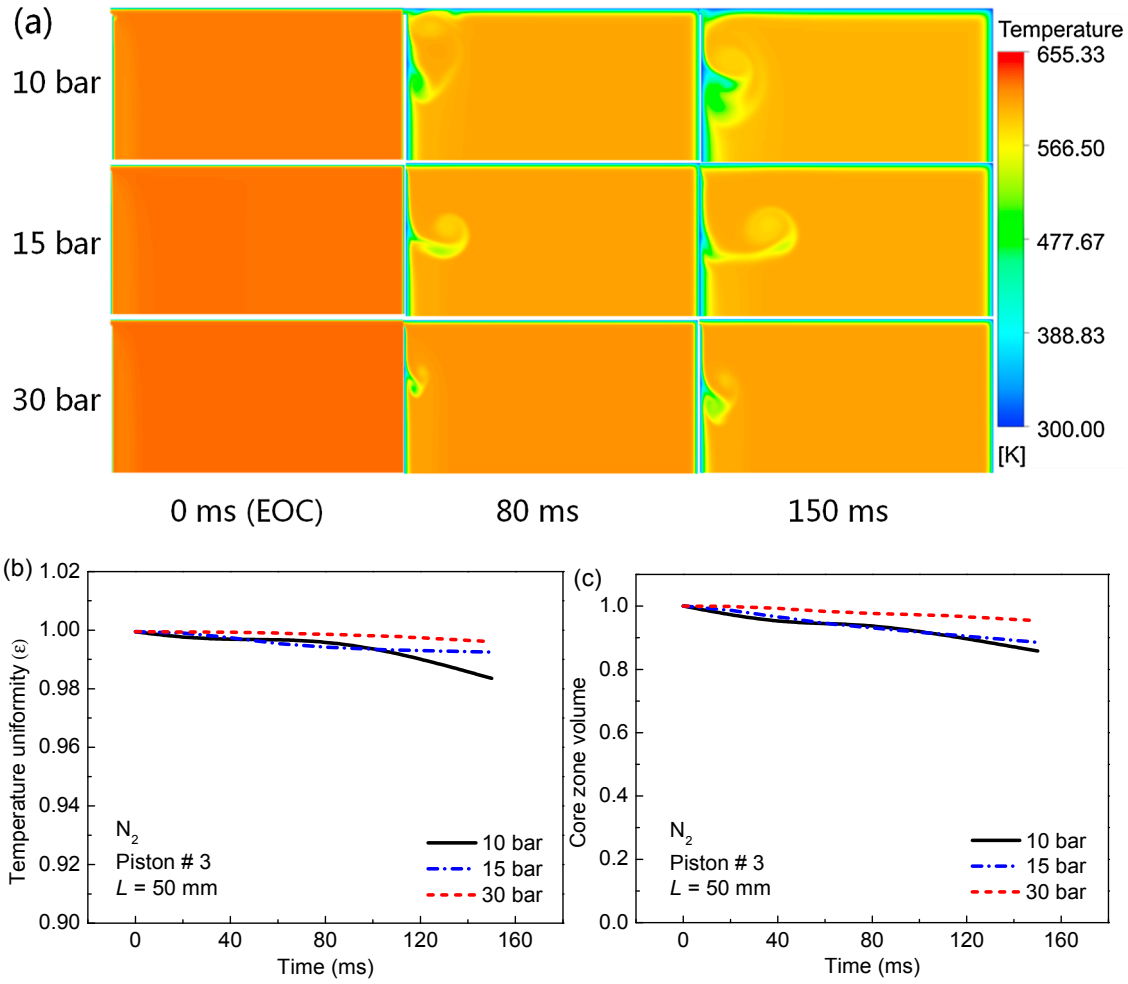

Fig. 7. (a) Temperature distributions for piston #3 at different times; (b) Temperature uniformity variable for piston #3 as a function of time; (c) Core zone volume for piston #3 as a function of time; P_C = 10, 15 and 30 bar; N_2; L = 50 mm.

shaped crevices are very close. Because "narrow and deep" crevice (#3) can reduce the total length of the whole RCM system in the axial direction, we then proposed that #3 creviced piston should be an optimized one for our rapid compression machine facility. As such, we further tested the performance of #3 piston against different inert gases, pressures and chamber lengths.

2.4.2. Test against different compression pressure

It should be also noted that the boundary layer effect becomes more prominent at relatively low pressures [19] and may possibly result in the deterioration of the temperature homogeneity. Since different pressure can lead to different temperature homogeneity in the reaction chamber [18,19], the temperature fields of piston #3 are further compared at the pressure of 10 and 30 bar, as shown in Fig. 7(a).

It can be seen that temperature distributions are less sensitive to pressure compared with the crevice volume. Increasing pressure has suppressed the development of vortex, leading to slight smaller scale of cold vortex and thus less mixing between the cold boundary layer gas and the hot core gas. Further comparisons of the ε and core zone volume are respectively shown in Fig. 7(b) and (c). Both the ε and core zone volume traces have shown that the discrepancies among different pressures are very small in a short period time after EOC. As time proceeds, cold gas disturbance gradually penetrates into the core zone and leads to the deterioration of the temperature homogeneity and shrink of core zone volume, and the discrepancies are increased. Another interesting result is that thermal boundary layer at 10 bar is obviously thicker than that at 15 bar. Additionally, the penetration distance of the cold disturbance gas is shorter at 10 bar than 15 bar. Overall, increasing pressure has shown promoting effect on temperature homogeneity, which is consistent with the previous work [19]. Piston #3 has shown a good performance under the all the pressure range investigated.

2.4.3. Test against different inert gases

In RCM experiments, temperature after compression can also be regulated by adjusting the proportion of Ar and N_2 and thus the C_p of the mixtures. The performance of the piston #3 is also tested against the different inert gases. The simulated temperature distributions in the reaction chamber are shown in Fig. 8(a). Due to the lower C_p of Ar, the maximum temperature in Ar is higher than 1000 K, and a good uniformity is achieved in the reaction chamber after EOC. Compared to that in N_2, as shown in Fig. 8(b) and (c), ε and core zone volume in Ar have smaller decreasing rate which is attributed to the lower thermal conductivity of Ar. Core zone volume in Ar is smaller than it in N_2 at EOC because of the higher temperature difference between the hot core gas and the cold disturbed gas. We note that there is only a slight drop of ε and core zone volume as a function of time, and they are still as high as 0.998 and 0.939 respectively at 150 ms, indicating that the buffer gas does not affect much of the temperature homogeneity, and piston #3 can perform even better for Ar dilution cases.

2.4.4. Test against different chamber length (compression ratio)

The present RCM adjusts its compression ratio by changing the length of the reaction chamber (L) to create different thermodynamic

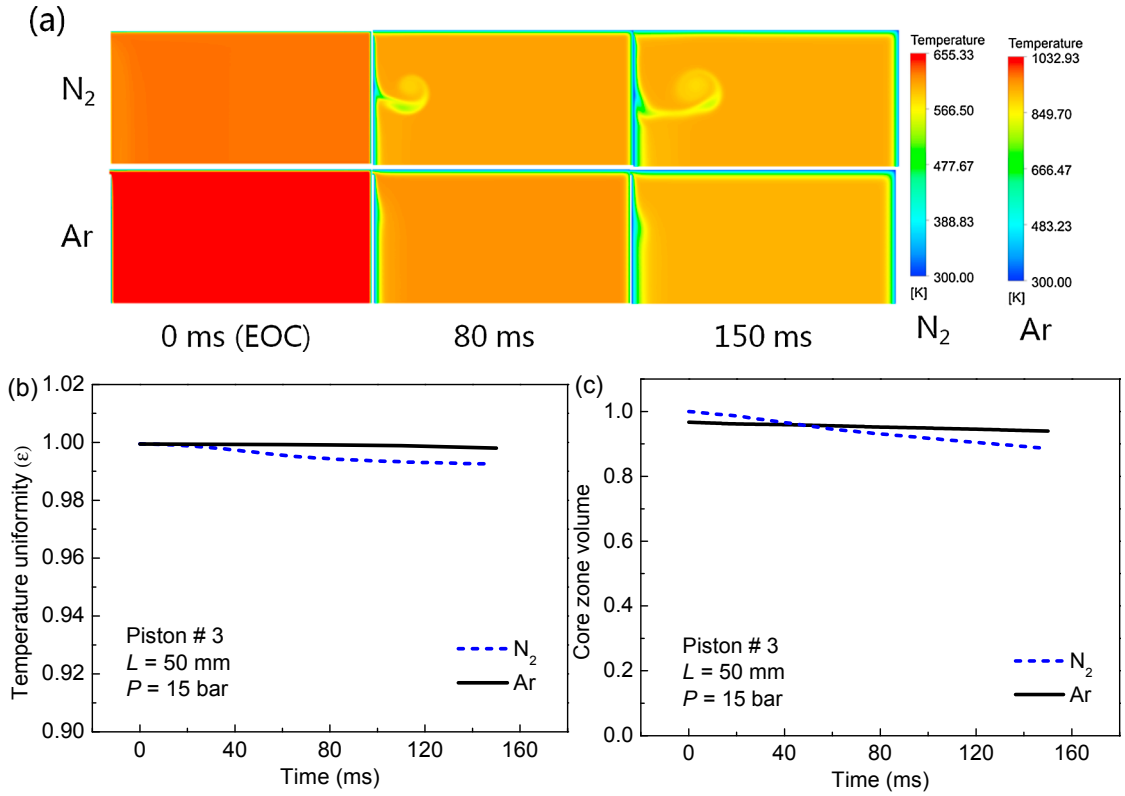

Fig. 8. (a) Temperature distributions (K) of #3 piston at 0, 80 and 150 ms, N_2 and Ar as the bulk gas. (b) Temperature uniformity variable for Ar and N_2 as a function of time; (c) core zone volume for Ar and N_2 as a function of time; P_c = 15 bar and L = 50 mm.

conditions for IDT determination. Therefore, simulations are also conducted for different chamber lengths (L = 30, 50 and 100 mm) under the same pressure (30 bar). Fig. 9(a) compares the temperature distributions of piston #3 for the case L = 30 mm, L = 50 mm and L = 100 mm. Due to increment of the compression ratio as L is decreased, the maximum temperature is increased in turn from the case L = 100 mm to L = 30 mm. Also, it is seen that under all the chamber length cases, piston #3 still shows good temperature uniformity performance in the reaction chamber, and only limited disturbance was generated in front of the piston head in L = 100 and 50 mm, and most of the hot gas remain unaffected. The scale of disturbance is larger in longer L cases, however, there are also more unaffected gas in longer L cases which will improve the total temperature uniformity in the reaction chamber at the same time. The effect of chamber length on the temperature uniformity is presented in Fig. 9(b). ε for longer L is slightly lower through the whole simulation process. However, ε is still as high as 0.994 at 150 ms for L = 100 mm, indicating that the cold gas disturbance has weak influence on overall temperature homogeneity. The core zone volume histories of different chamber length cases are also very close through the entire period, as shown in Fig. 9(c). This result has confirmed the recommendations of Park and Keck [35], but is contradictory to the conclusion of Mittal et al. [19]. The chamber length studied by Mittal et al. is ranged from 14 to 28 mm, which is shorter than the minimum L in this study. Except for the difference in length scale, the temperature distributions compared in reference [19] are all influenced by roll-up vortex, and smaller L will enhance the mixing between cold boundary layer and hot core region, and thus lead to the contradictory conclusion. The above discussion indicates that piston #3 will achieve good temperature uniformity performance and core zone volume for different compression ratio and yield good thermodynamic conditions in the RCM for IDT determination.

The above numerical simulation provides some guidance for crevice piston optimization. Because the temperature homogeneity deteriorates with time as a result of the vortex transportation in the reaction chamber, the crevice volume should be large enough to contain most of the boundary layer gas during compression so as to ensure that no vortex is formed at EOC. Otherwise, this cold gas disturbance mixes with the hot core region charge and induces significant temperature inhomogeneity and even causes the failure of the adiabatic core hypothesis. Crevice volume ratio $V_{cr}/\pi R^2 S$ = 0.02 is used in this RCM, and more crevice volume ratio of other RCMs available are provided in Supplementary materials for comparison. In addition, the different shapes of crevice with enough large crevice volume do not influence the temperature homogeneity in the reaction chamber, though it does affect the cold charge in the crevice volume. With a better design of the piston crevice geometry, it is supposed to reduce the gas mixing in the reaction chamber and thus lead to lower cooling rate after compression. However, using larger piston crevice especially that with high aspect ratio will also induce more heat loss and thus will increase the cooling rate of the entire charge.

Piston #3 has exhibited high temperature homogeneity and core zone volume in wide ranges of pressure, insert gases and reaction chamber length, even though small disturbances are not totally removed under certain conditions. Further increasing the crevice volume will only show limited promotion and it will decrease the maximum compression ratio due to increased clearance volume at EOC and induce more complex influence on the multi-staged ignition process [19]. Therefore, an optimized creviced piston structure (# 3) is considered and proposed in our rapid compression machine facility.

3. Validation of rapid compression machine

3.1. Specifications of experimental facility

Based on the above consideration, a new RCM was built in our lab. The schematic of this RCM is shown in Fig. 10. Six components comprise the apparatus: the high-pressure tank, the driving chamber, the hydraulic chamber with oil, the compression chamber, the combustion

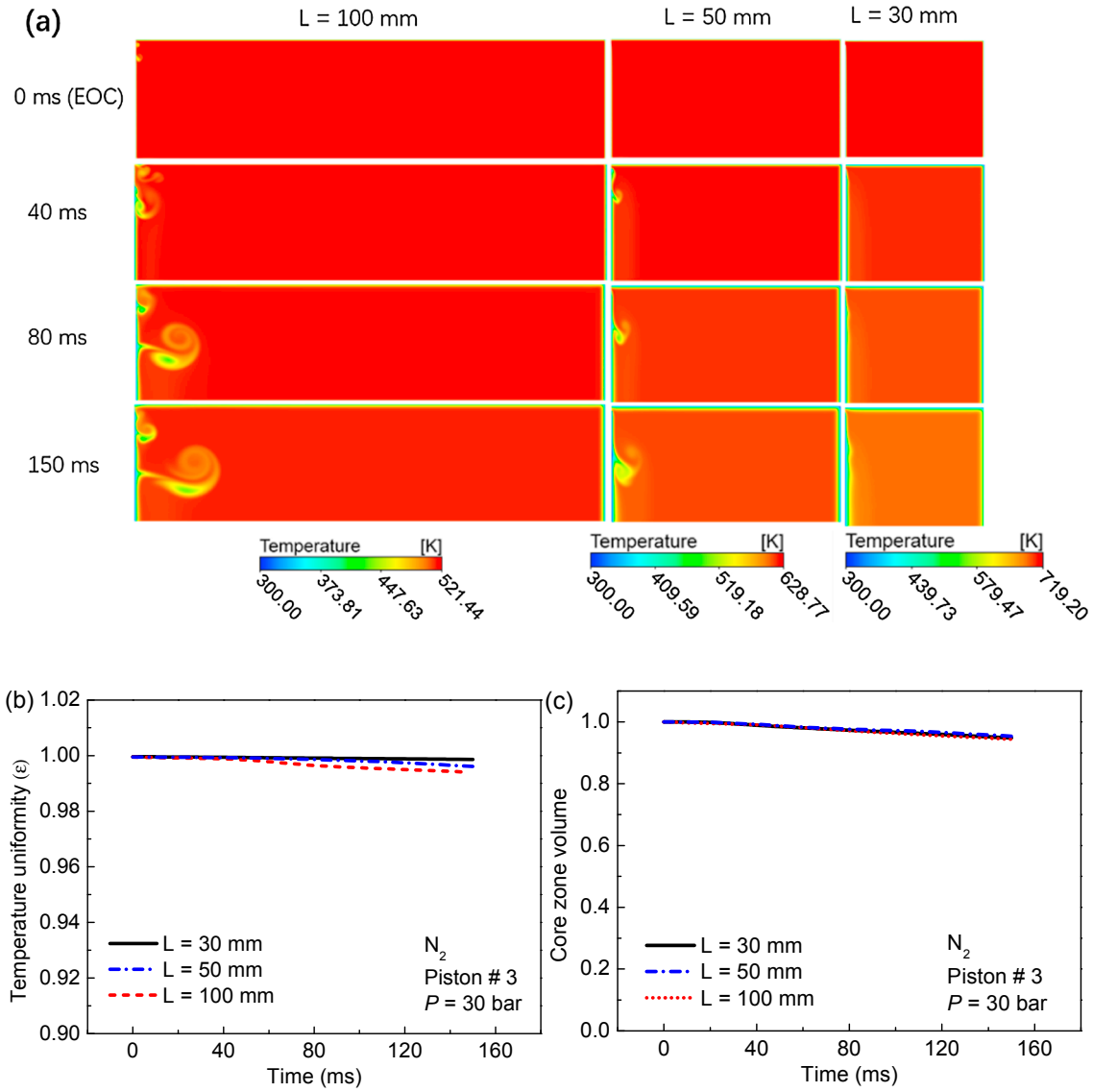

Fig. 9. (a) *Pc* = 30 bar; temperature distributions (K) of piston #3 for reaction chamber length of 30, 50 and 100 mm at different times. (b) ε of piston #3 for different reaction chamber lengths; (c) core zone volume of piston #3 for different reaction chamber lengths; N_2 as the bulk gas.

chamber, and the control and data acquisition system. We note that because the numerical simulation in Section 2 indicates that crevice #3 is an optimized piston due to its minimized temperature non-uniformity, in our experiment, we used # 3 piston with different compression ratio to achieve different temperature condition for IDT measurements.

The high-pressure tank is charged with air and maintained at a constant pressure before compression. The compressed surface area of piston in the compression chamber is 16 times to that in the compression chamber, so that much higher pressure in the combustion chamber can be achieved by using only a small driving pressure. After the compression, pneumatic force on the driving chamber will also hold the pistons in their position. By adjusting the driving pressure in the tank, compression speed can be changed. However, the maximum driving pressure is limited both by mechanical vibration and the hydraulic pressure. Before the compression, the hydraulic chamber is fully filled with high pressure oil to lock the pistons at their resting position while the pneumatic force is on. The compression is then triggered by releasing the oil through a solenoid valve and, in the meantime, the data acquisition system begins to record the raw pressure signal. The compression chamber of this RCM has a bore (D) of 50.8 mm and stroke length (S) of 332 mm. The creviced piston based on CFD optimization is adopted to prevent the mixing of boundary and core region due to the roll up vortex, such that satisfactory thermal homogeneity is ensured. Details of the CFD optimization are discussed in Section 2. The length of the combustion chamber can be changed from 20 to 100 mm at the step of 1 mm, so that different volume compression ratios and the resulting temperature can be achieved. The pressure inside the combustion chamber is monitored using a recess-mounted piezoelectric pressure transducer (Kistler 6125C) combined with a charge amplifier (Kistler 5018A). Pressure is recorded by a National Instrument USB-6361 data collecting card running at a frequency of 100 kHz.

Testing mixtures, the reactive mixture and the non-reactive mixture, are respectively prepared in two mixing-vessels according to their partial pressures and the partial pressures of the liquid components are kept blow at least 1/2 of its saturated vapor pressure to avoid condensation. An OMEGA DPG4000 with a pressure range of 3 bar is used to measure the pressure in mixing-vessel and the initial pressure in the combustion chamber. Ar and N_2 are used as the dilution gas and C_p of the mixture is adjusted by adjusting the proportions of Ar and N_2. The experiments are conducted at least an hour later to ensure the homogeneity of the mixtures.

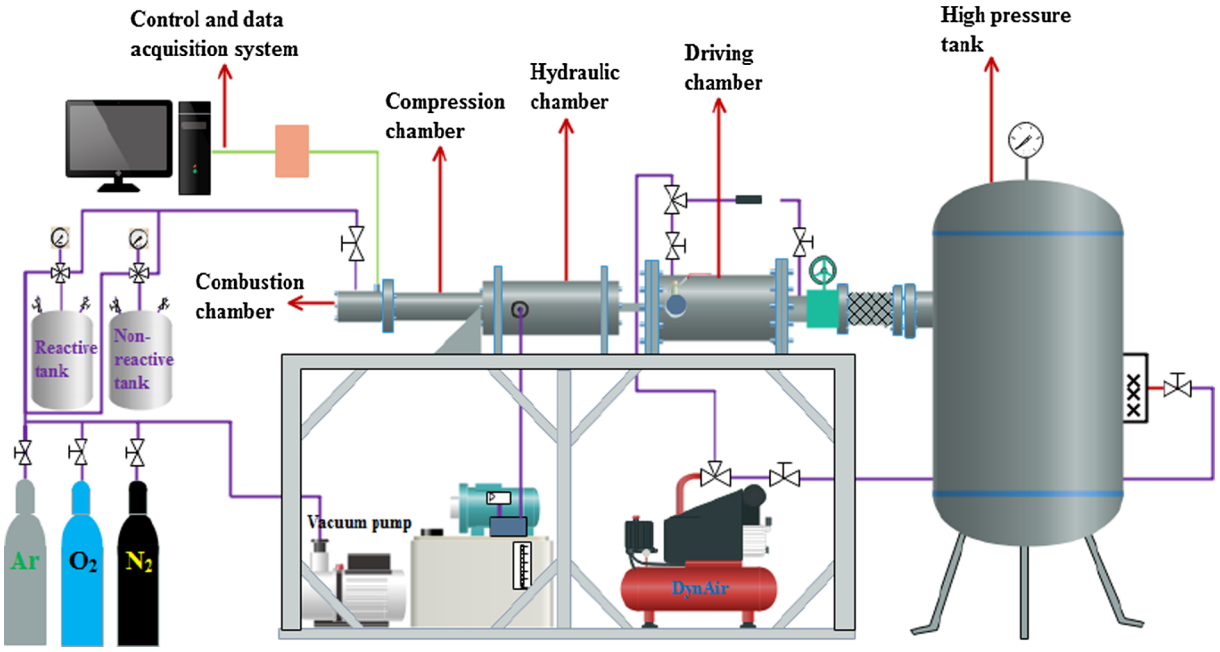

Fig. 10. Schematic of experimental facility of the present RCM.

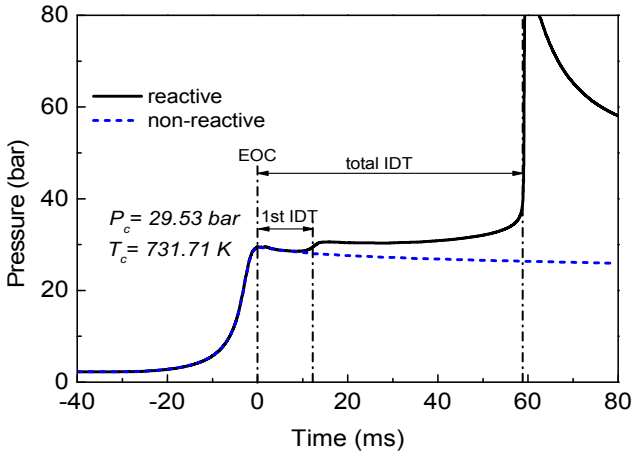

Fig. 11. Typical measured pressure evolution history and the definition of 1st and total IDT (mixture of toluene (64.0%), n-heptane (14.5%) and iso-octane (21.5%), equivalence ratio = 1.0, dilution ratio = 12.3).

For typical mixtures with typical two stage ignition behavior, both the first-stage ignition delay (1st IDT) in case of two-stage ignition, and total ignition delay (total IDT) corresponding to the main ignition can be deduced from pressure traces and defined as the time intervals between EOC and the steepest pressure rise (dP/dt) of the 1st stage and the second stage pressure rise, as shown in Fig. 11. EOC is chosen at the point where the pressure reaches to a peak (P_{max}) before ignition. Although the piston may not actually stop there, the time difference could be ignored.

In the 0-dimentional reacting flow simulation, volume history profile [36,37] is adopted to account for the facility effect. The volume history profile of a certain compression is deduced from the corresponding non-reactive pressure trace, which replaces O_2 by N_2 in the mixture. Based on "adiabatic core" assumption, heat loss is ignored in the volume history profile. The changing volume in each time point is calculated as Eq. (4). With the input parameter of P_0 and T_0, the volume history profile can well depict the environment of the core zone in the reaction chamber. Therefore, accurate measurements of non-reactive pressure trace are also very crucial in validating a kinetic model.

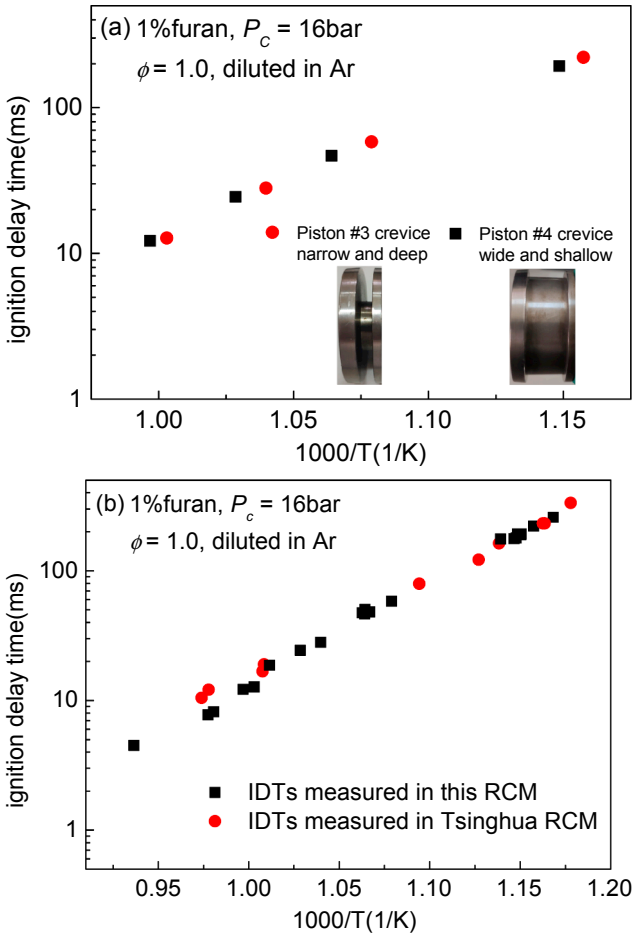

Fig. 12. IDTs of the stoichiometric furan/Ar/O_2 mixture, P_C = 16 bar, (a) using both piston #3 (circle) and #4 (square); (b) IDTs measured using the present RCM and the Tsinghua RCM (Refer to [7] for details of Tsinghua RCM).

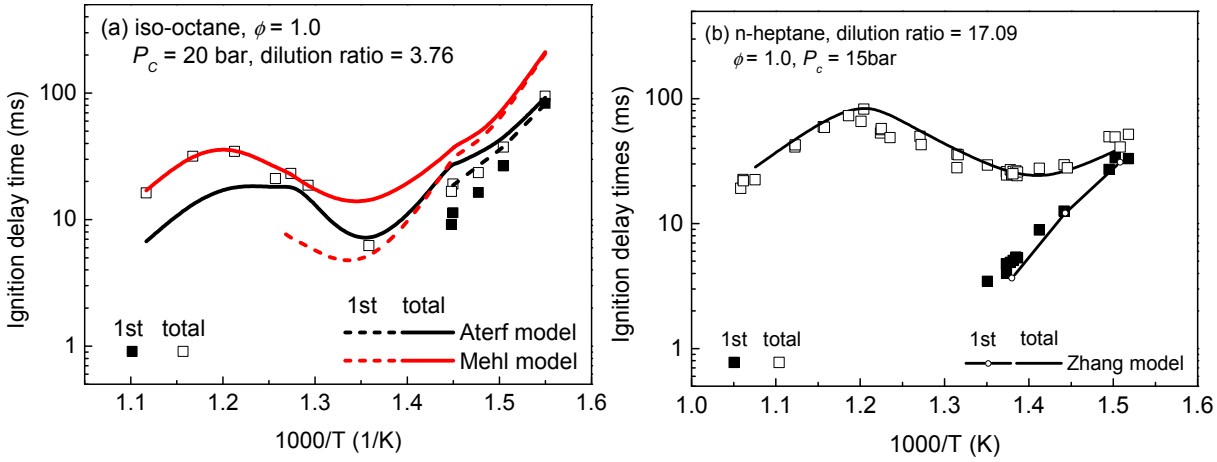

Fig. 13. Measured and predicted IDT of typical mixtures with two stage ignition behavior stoichiometric iso-octane/N_2/Ar/O_2 mixture, dilution ratio 3.76; P_C = 20 bar; stoichiometric n-heptane/Ar/O_2 mixture, dilution ratio 17.1; P_C = 15 bar.

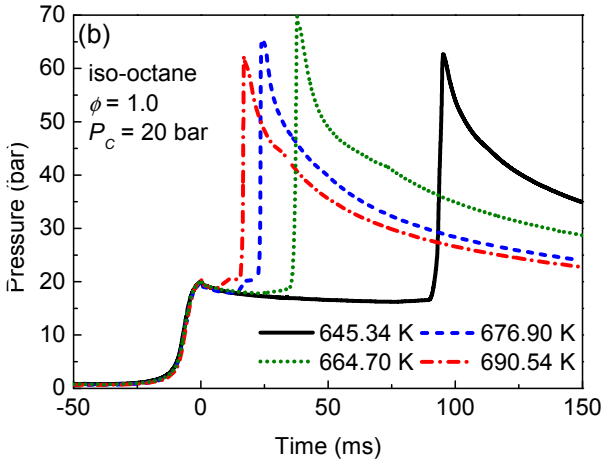

Fig. 14. Pressure traces of iso-octane mixture at different temperatures measured in this RCM; stoichiometric iso-octane mixtures, dilution ratio = 3.76 and P_C = 20 bar.

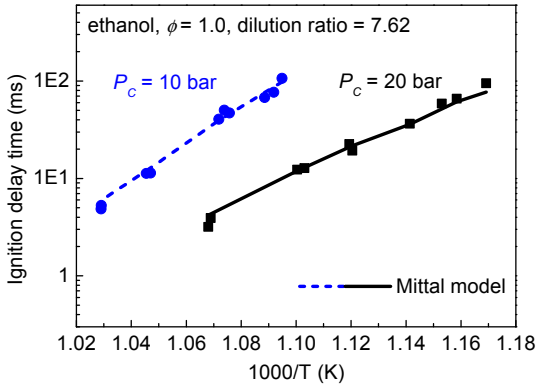

Fig. 15. IDTs of the stoichiometric ethanol mixture at P_c = 10 and 20 bar, scatters are the experimental data measured in this RCM, lines are model predictions of Mittal et al.[42].

$$V(t) = V_0\left(\frac{P_0}{P(t)}\right)^{\frac{1}{\gamma}} \quad (4)$$

3.2. Ignition delay time measurement with the optimized piston design

We first experimentally tested the effect of the crevice shape on the IDT measurements, as shown in Fig. 12(a). The "narrow and deep crevice" piston #3 and the "wide and shallow crevice" piston #4 show very consistent measured values of the ignition delay times for given mixture condition. In addition, we also compared the present measurements with the data from the Tsinghua University RCM because of the very similar structure of these two RCMs, as shown in Fig. 12(b). Results show that the IDT data is very consistent for this mixture on these two RCMs.

3.3. Comparison of the present RCM data with kinetic model predictions and other RCMs

3.3.1. Mixtures with the negative temperature coefficient (NTC) behavior

The measured IDTs of mixtures (iso-octane and n-heptane) with typical NTC behaviors are presented in Fig. 13. Two iso-octane models were adopted in the IDTs simulation for iso-octane, including the Atef model [38] and the Mehl model [39]. The Mehl model has been validated by comparison to experiments in shock tubes and rapid compression machines. The Atef model has been updated based on the Mehl model and further compared against IDTs, jet-stirred reactor oxidation speciation data, premixed laminar flame speeds, counterflow diffusion

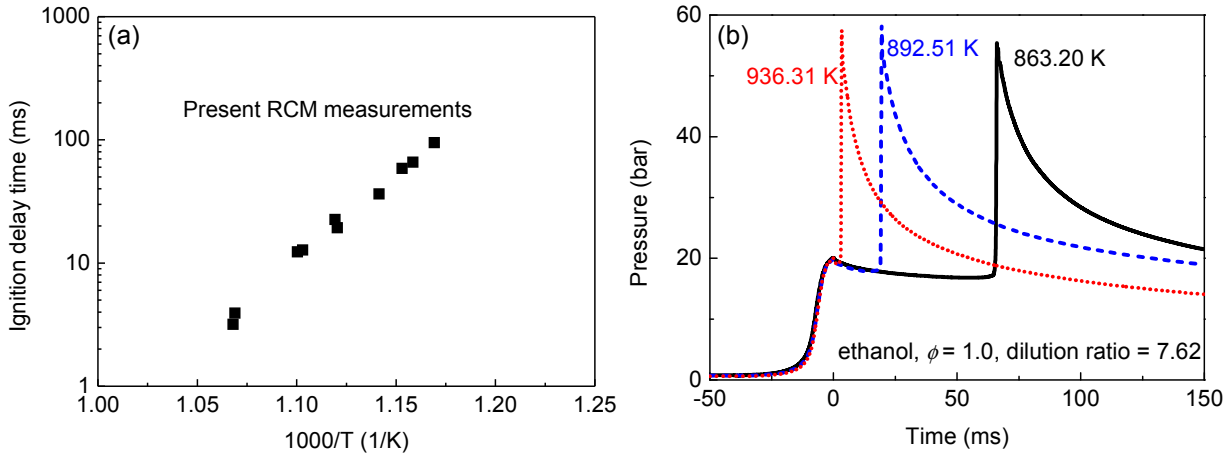

Fig. 16. Typical measured ignition delay times of stoichiometric ethanol mixtures for dilution ratio of 3.76 at 20 bar, using the present RCM. (b) Pressure traces of ethanol mixture at different temperatures measured in this RCM; stoichiometric ethanol mixtures, dilution ratio = 3.76 and P_C = 20 bar.

flame ignition, and shock tube pyrolysis speciation data available in the literature. We note that the numerical simulation of the IDT has taken into account the facility effect by considering the volume history profiles.

The model predictions have shown great similarity as those in the literature [38]. Generally, the Mehl model shows better agreement with the experimental data in the high temperature range, while the prediction of the Atef model is slightly lower. However, in lower temperature range, the Atef model shows better prediction, while the Mehl model slightly underestimates the reactivity.

The IDTs of stoichiometric n-heptane/Ar/O_2 mixture, at the dilution ratio of 17.09, were measured at 15 bar by using this RCM, as shown in Fig. 13(b). The IDTs predictions were simulated using volume history method and the recent n-heptane kinetic model of Zhang et al. [40] is adopted, which has been validated against IDTs, jet stirred reactor specifies profiles and laminar speed over a wide range of conditions. The model prediction generally shows good agreement with the 1st and total IDTs measurement and has well captured the NTC ignition behavior of the n-heptane mixtures.

Recognizing that these two models have been extensively validated against experimental data, this level of agreement with of the present experimental measurements indicates that the IDTs measured in this RCM are reliable in validating the kinetic models of the mixtures with typical two stage ignition behavior.

Direct comparison of IDT measurements from different RCMs is challenging because of the different facility effect, such as the compression and heat loss characteristics. IDTs of iso-octane mixtures had been compared in 2nd international RCM workshop [5] and therefore are also compared here with the measurement of this RCM just for reference, as shown by Fig. 14(a). It should be noted that, although the dilution ratio is fixed as 3.76, different insert gases, such as Ar, CO_2 and N_2, were used in the measurement and further information of the mixture components can be found in reference [5,38]. Over all, the IDTs measured in this RCM have shown consistent NTC behavior and values with that in other RCMs especially NUIG in both low and high temperature range.

Pressure traces of iso-octane mixture at different temperatures measured in this RCM are shown in Fig. 14(b). Pressure traces have shown consistent compression process and well captured the one or two staged ignition behaviors of iso-octane.

3.3.2. Mixtures without NTC behaviors

Ethanol has recently been suggested to be a candidate fuel for standard data collection in RCMs because it has simple chemistry and does not cause device specific issues due to multistage heat release [41]. As such we also select ethanol as the target fuel by using our new RCM facility. As shown in Fig. 15, the IDTs of stoichiometric ethanol mixture with dilution ratio of 7.62 under two pressures were measured in this RCM. It is seen that the measured IDT in logarithm of this mixture at two pressures show clearly linear dependence on the inverse temperature, and higher pressure reduces the ignition delay times significantly. Chemical kinetic model of ethanol in [42] was used in the simulation. This model has been validated against their measured autoignition characteristics of ethanol at low temperatures and elevated pressures. The model predictions also show good agreement with the present experimental data under both pressures and the model performance is also similar to that in reference [42].

The combustion community has organized series of RCM workshops for improving understanding of the RCM measurements [43], and ethanol is typically selected as the fuel because of its relatively well understood chemistry. We also presented ignition delay times measurements of ethanol at typical conditions, using the present RCM, as shown in Fig. 16(a). Pressure traces of ethanol mixture at different temperatures measured in this RCM are also shown in Fig. 16(b) for reference.

Details of the mixtures composition, IDTs measurement and the volume history profiles are provided in the Supplementary material.

3.3.3. Uncertainty analysis

Uncertainty in the IDT measurement from an RCM includes the uncertainty in P_C, T_C and reactant composition [4,5]. The uncertainty in pressure arises from in initial pressure measurement, pressure transducer, and charge amplifier. The uncertainty in temperature comes from the initial temperature measurement and pressure profile ($P(t)$) because the temperature history is deduced from $P(t)$ based on "adiabatic core" hypothesis. The uncertainty in measuring the reactant composition will also contribute to the uncertainty in temperature by changing the thermodynamics of the mixture. When plotting the IDTs in a reported P_C and T_C, the uncertainties of T_C are usually given for each data point. By using the independent parameters methodology as described in reference [44], the uncertainty in T_C is estimated to be less than 8 K for all the experimental data in this study. Details of the uncertainty in T_C are provided in the Supplementary material.

4. Conclusion

As a widely-used experimental facility for studying fuel autoignition in the low-to-intermediate temperatures, rapid compression machine (RCM) is designed to create a homogenous reaction system under a certain initial temperature and pressure, which can hence be modeled and analyzed as a 0-dimensional thermochemical system immune to the intervention of heat and mass transfer. In reality, the unavoidable flow

motion and heat loss deviate the RCM system from being completely homogeneous. Consequently, the existence and the temporal and spatial characteristics of an “adiabatic core” are vital to a successful design and operation of RCM. The focus of the present work was to investigate, optimize, establish, and validate a crevice piston design for promoting the “adiabatic core” validity in RCM. We first computationally investigated the influences of the crevice volume and shape effect on the “adiabatic core” validity by examining the temperature distribution in the combustion chamber. Results show that the crevice volume should be large enough to contain the boundary layer gas during the compression process and no vortex should be formed at EOC. Crevice shape has minimized influence on the reaction chamber temperature homogeneity according to both the simulation and experimental result. As such, an optimized piston structure was proposed and tested against wide range of pressure, insert gas and reaction chamber length. Larger scale of disturbance has been found using longer reaction chambers and using argon as insert gas will lead to more uniform temperature distribution. Further, this optimized piston was adopted in the newly build RCM system. Ignition delay time measurements using this new RCM were compared with the experimental data using other RCM and also with the numerical predictions obtained by using several well recognized and validated kinetic models for fuels with/without negative temperature coefficient behavior. The results have confirmed the validity of the present RCM for investigation of the auto-ignition characteristics of various mixtures in the low-to -intermediate temperature.

Acknowledgements

This work is supported by the National Natural Science Foundation of China (51722603 and 91541107), the Science Challenging Program (TZ2016001), and the Fundamental Research Funds for the Central Universities. The work at the Hong Kong Polytechnic University was supported by NSFC (No. 91641105) and additionally by the university (4-BCE8).

Appendix A. Supplementary data

Supplementary data to this article can be found online at https://doi.org/10.1016/j.fuel.2019.04.030.

References

[1] Hanson RK, Davidson DF. Recent advances in laser absorption and shock tube methods for studies of combustion chemistry. Prog Energy Combust Sci 2014;44:103–14.
[2] Tang C, Man X, Wei L, Pan L, Huang Z. Further study on the ignition delay times of propane–hydrogen–oxygen–argon mixtures: Effect of equivalence ratio. Combust Flame 2013;160(11):2283–90.
[3] Tang C, Wei L, Man X, Zhang J, Huang Z, Law CK. High temperature ignition delay times of C5 primary alcohols. Combust Flame 2013;160(3):520–9.
[4] Sung C-J, Curran HJ. Using rapid compression machines for chemical kinetics studies. Prog Energy Combust Sci 2014;44:1–18.
[5] Goldsborough SS, Hochgreb S, Vanhove G, Wooldridge MS, Curran HJ, Sung CJ. Advances in rapid compression machine studies of low- and intermediate-temperature autoignition phenomena. Prog Energy Combust Sci 2017;63:1–78.
[6] Xu N, Wu Y, Tang C, Zhang P, He X, Wang Z, et al. Experimental study of 2,5-dimethylfuran and 2-methylfuran in a rapid compression machine: Comparison of the ignition delay times and reactivity at low to intermediate temperature. Combust Flame 2016;168:216–27.
[7] Di H, He X, Zhang P, Wang Z, Wooldridge MS, Law CK, et al. Effects of buffer gas composition on low temperature ignition of iso-octane and n-heptane. Combust Flame 2014;161(10):2531–8.
[8] Xu N, Wu Y, Tang C, Zhang P, He X, Wang Z, et al. Ignition delay times of low alkylfurans at high pressures using a rapid compression machine. Proc Combust Inst 2017;36:323–32.
[9] Davidson DF, Hanson RK. Interpreting shock tube ignition data. Int J Chem Kinet Kinetics 2004;36(9):510–23.
[10] Ji W, Zhang P, He T, Wang Z, Tao L, He X, et al. Intermediate species measurement during iso-butanol auto-ignition. Combust Flame 2015;162(10):3541–53.
[11] Barrazabotet CL, Wagnon SW, Wooldridge MS. On the combustion chemistry of ethanol: ignition and speciation studies in a rapid compression facility. J Phys Chem A 2016;120:7408–18.
[12] Minetti R, Carlier M, Ribaucour M, Therssen E, Sochet LR. A rapid compression machine investigation of oxidation and auto-ignition of n-Heptane: measurements and modeling. Combust Flame 1995;102(3):298–309.
[13] Griffiths JF, Hughes KJ, Porter R. The role and rate of hydrogen peroxide decomposition during hydrocarbon two-stage autoignition. Proc Combust Inst 2005;30(30):1083–91.
[14] Hu H, Keck J. Autoignition of adiabatically compressed combustible gas mixtures. SAE Technical Paper 872110; 1987.
[15] Lee D, Hochgreb S. Rapid compression machines: heat transfer and suppression of corner vortex. Combust Flame 1998;114(114):531–45.
[16] Wurmel J, Simmie J. CFD studies of a twin-piston rapid compression machine. Combust Flame 2005;141(4):417–30.
[17] Mittal G, Sung CJ. Aerodynamics inside a rapid compression machine. Combust Flame 2006;145(1–2):160–80.
[18] Mittal G, Raju MP, Sung CJ. Computational fluid dynamics modeling of hydrogen ignition in a rapid compression machine. Combust Flame 2008;155(3):417–28.
[19] Mittal G, Raju MP, Sung CJ. Vortex formation in a rapid compression machine: influence of physical and operating parameters. Fuel 2012;94(1):409–17.
[20] Goldsborough SS, Mittal G, Banyon C. Methodology to account for multi-stage ignition phenomena during simulations of RCM experiments. Proc Combust Inst 2013;34(1):685–93.
[21] Mittal G, Bhari A. A rapid compression machine with crevice containment. Combust Flame 2013;160(12):2975–81.
[22] Mittal G, Chomier M. Effect of crevice mass transfer in a rapid compression machine. Combust Flame 2014;161(2):398–404.
[23] Bourgeois N, Jeanmart H, Winckelmans G, Lamberts O, Contino F. How to ensure the interpretability of experimental data in Rapid Compression Machines? A method to validate piston crevice designs. Combust Flame 2018;198:393–411.
[24] Yousefian S, Gauthier F, Moránguerrero A, Richardson RR, Curran HJ, Quinlan NJ, et al. A simplified approach to the prediction and analysis of temperature inhomogeneity in rapid compression machines. Energy Fuels 2015;29:216–25.
[25] ANSYS ICEM CFD® Academic Research, Release 18.2. ANSYS, Inc.
[26] ANSYS Fluent® Academic Research, Release 18.2. ANSYS, Inc.
[27] Yousefian S, Quinlan NJ, Monaghan RFD. Simulation of turbulent flow in a rapid compression machine: large Eddy Simulation and computationally efficient alternatives for the design of ignition delay time experiments. Fuel 2018;234:30–47.
[28] Sutherland W. The viscosity of gases and molecular force. Philos Mag 1893;36:507–31. Edinburgh.
[29] Griffiths JF, MacNamara JP, Mohamed C, Whitaker BJ, Pan JF, Sheppard CGW. Temperature fields during the development of autoignition in a rapid compression machine. Faraday Discuss 2001;119:287–303.
[30] Clarkson J, Griffiths JF, MacNamara JP, Whitaker BJ. Temperature fields during the development of combustion in a rapid compression machine. Combust Flame 2001;125(3):1162–75.
[31] Strozzi C, Mura A, Sotton J, Bellenoue M. Experimental analysis of propagation regimes during the autoignition of a fully premixed methane–air mixture in the presence of temperature inhomogeneities. Combust Flame 2012;159(11):3323–41.
[32] Strozzi C, Sotton J, Mura A, Bellenoue M. Experimental and numerical study of the influence of temperature heterogeneities on self-ignition process of methane-air mixtures in a rapid compression machine. Combust Sci Technol 2008;180(10–11):1829–57.
[33] Pan J, Hu Z, Wei H, Pan M, Liang X, Shu G, et al. Understanding strong knocking mechanism through high-strength optical rapid compression machines. Combust Flame 2019;202:1–15.
[34] Pan J, Wei H, Shu G, Chen Z, Zhao P. The role of low temperature chemistry in combustion mode development under elevated pressures. Combust Flame 2016;174:179–93.
[35] Park P, Keck J. Rapid compression machine measurements of ignition delays for primary reference fuels. SAE Technical Paper 900027; 1990.
[36] Sarathy SM, Park S, Weber BW, Wang W, Veloo PS, Davis AC, et al. A comprehensive experimental and modeling study of iso-pentanol combustion. Combust Flame 2013;160(12):2712–28.
[37] Weber BW, Sung C-J. Comparative autoignition trends in butanol isomers at elevated pressure. Energy Fuels 2013;27(3):1688–98.
[38] Atef N, Kukkadapu G, Mohamed SY, Rashidi MA, Banyon C, Mehl M, et al. A comprehensive iso-octane combustion model with improved thermochemistry and chemical kinetics. Combust Flame 2017;178:111–34.
[39] Mehl M, Pitz WJ, Westbrook CK, Curran HJ. Kinetic modeling of gasoline surrogate components and mixtures under engine conditions. Proc Combust Inst 2011;33(1):193–200.
[40] Zhang K, Banyon C, Bugler J, Curran HJ, Rodriguez A, Herbinet O, et al. An updated experimental and kinetic modeling study of n- heptane oxidation. Combust Flame 2016;172:116–35.
[41] Stephen Dooley AH, Farooq Aamir, Vanhove Guillaume, Goldsborough Scott. Standard data collection for RCMs-2nd rapid compression machine characterization initiative. International RCM Workshop. 2018.
[42] Mittal G, Burke SM, Davies VA, Parajuli B, Metcalfe WK, Curran HJ. Autoignition of ethanol in a rapid compression machine. Combust Flame 2014;161(5):1164–71.
[43] Federico Ferliga SD, Horward M, Leahy L, Comandini A, Farooq A, Heufer A, et al. Rapid compression machine workshop 2ND characterization initiative – ethanol ignition. 37th International Symposium on Combustion. 2018. Ireland, Dublin.
[44] Weber BW, Sung CJ, Renfro MW. On the uncertainty of temperature estimation in a Rapid Compression Machine. Combust Flame 2015;162(6):2518–28.